Structure
Article

Large-Scale Conformational Flexibility Determines the Properties of AAA+ TIP49 ATPases

Michael Petukhov,[1,3] Adilia Dagkessamanskaja,[4,5] Martin Bommer,[6,8] Tracey Barrett,[6] Irina Tsaneva,[7] Alexander Yakimov,[1,3] Richard Quéval,[4,5] Alexey Shvetsov,[1,3] Mikhail Khodorkovskiy,[2] Emmanuel Käs,[4,5,*] and Mikhail Grigoriev[2,4,5,*]
[1]Department of Biophysics
[2]Institute for Nanobiotechnologies
Saint Petersburg State Polytechnical University, Saint Petersburg 197376, Russia
[3]Division of Molecular and Radiation Biophysics, Petersburg Nuclear Physics Institute, National Research Centre Kurchatov Institute, Gatchina 188300, Russia
[4]Unité Mixte de Recherche 5099, Centre National de la Recherche Scientifique
[5]Université Paul Sabatier,Université de Toulouse
Laboratoire de Biologie Moléculaire Eucaryote, 31000 Toulouse, France
[6]Department of Biological Sciences, Institute of Structural Molecular Biology, Crystallography, Birkbeck College, London E11 4HL, UK
[7]Institute of Structural and Molecular Biology, University College London, London WC1E 6BT, UK
[8]Present address: Strukturbiologie-Gruppe, Haus 18, Institut für Biologie, Philippstrasse 13, Berlin 10115, Germany
*Correspondence: kas@ibcg.biotoul.fr (E.K.), grigor@ibcg.biotoul.fr (M.G.)
http://dx.doi.org/10.1016/j.str.2012.05.012

SUMMARY

The TIP49a and TIP49b proteins belong to the family of AAA+ ATPases and play essential roles in vital processes such as transcription, DNA repair, snoRNP biogenesis, and chromatin remodeling. We report the crystal structure of a TIP49b hexamer and the comparative analysis of large-scale conformational flexibility of TIP49a, TIP49b, and TIP49a/TIP49b complexes using molecular modeling and molecular dynamics simulations in a water environment. Our results establish key principles of domain mobility that affect protein conformation and biochemical properties, including a mechanistic basis for the downregulation of ATPase activity upon protein hexamerization. These approaches, applied to the *lik*-TIP49b mutant reported to possess enhanced DNA-independent ATPase activity, help explain how a three-amino acid insertion remotely affects the structure and conformational dynamics of the ATP binding and hydrolysis pocket while uncoupling ATP hydrolysis from DNA binding. This might be similar to the effects of conformations adopted by TIP49 heterohexamers.

INTRODUCTION

Within the broad AAA+ (ATPases Associated with diverse cellular Activities) superfamily, TIP49a and TIP49b form a taxonomic cluster that is singularly distant from other members, suggesting that these essential proteins possess unique properties (Ammelburg et al., 2006). TIP49 proteins are conserved through evolution and related to each other by sharing, in the case of human TIP49a and TIP49b, 42% identity. Despite this level of identity, TIP49 proteins exert different and often nonoverlapping molecular functions in vivo (Huen et al., 2010). Available data suggest that, at the molecular level, TIP49 proteins form oligomers ranging from dimers to dodecamers (Cheung et al., 2010; Gribun et al., 2008; Ikura et al., 2000; Niewiarowski et al., 2010; Puri et al., 2007; Torreira et al., 2008) and slowly unwind DNA in an ATP-dependent manner (Gorynia et al., 2011; Gribun et al., 2008; Papin et al., 2010; Wang et al., 2011). These properties might be important to bring about the conformational changes presumably required for a broad variety of biological processes including DNA repair, chromatin remodeling, histone exchange reactions, telomerase holoenzyme assembly, mitotic spindle formation, snoRNP biogenesis, and as yet unknown cellular pathways (Grigoletto et al., 2011; Huen et al., 2010; Jha and Dutta, 2009).

The crystal structure of hexameric TIP49a bound to ADP has been solved by Matias et al. (2006). TIP49a monomers contain 14 α helices, 16 β strands, and two 3_{10} helices and are organized into 3 structural domains: D1 (mostly N terminal), D2 (imbedded within the primary sequence of D1), and D3 (C terminal). Domains D1 and D3 form an ATP binding and hydrolysis module characteristic of the classical AAA+ fold and provide intersubunit interfaces involved in oligomerization (Erzberger and Berger, 2006; Matias et al., 2006). The central channel of the hexamer has a diameter of about 18 Å and is thought to be capable of accommodating a translocating single- but not double-stranded DNA molecule. Both TIP49a and TIP49b contain conserved Walker A and Walker B motifs involved in ATP binding and hydrolysis. Despite the presence of these important structural elements, the DNA-dependent ATPase activity of TIP49 proteins was found to be very low (Gribun et al., 2008; Papin et al., 2010) but increased in heteromeric complexes (Gorynia et al., 2011; Ikura et al., 2000; Puri et al., 2007). Weak ATPase activity can be attributed to very low ADP solvent accessibility in the protein active site, preventing its exchange with ATP within the TIP49a hexamer (Matias et al., 2006). More recently, the report of the crystal structure of mixed TIP49a/TIP49b heterohexamers

(Gorynia et al., 2011) and comparison to TIP49a crystals (Matias et al., 2006) have helped uncover details of the complexes at atomic resolution. These results show that TIP49a and TIP49b can substitute for one another within multimeric complexes without significant distortion of neighboring protein subunits.

In TIP49 proteins the Walker A and B boxes are separated by the insertion of the ~170 amino-acid (aa) D2 domain. The 3D structure of TIP49a reveals that this insert is folded as a distinct structural domain, which protrudes out of the hexameric ring and is connected to D1 via two flexible antiparallel β sheets (Matias et al., 2006). Although D2 shows no significant sequence similarity with other domains available in protein databases, parts of the TIP49a D2 sequence spanning residues 121–295 are structurally organized as an OB-fold domain (Oligonucleotide/oligosaccharide Binding) found in proteins involved in various aspects of nucleic acid metabolism (Murzin, 1993; Theobald et al., 2003; Walbott et al., 2010). In the case of human TIP49a, the OB-fold domain was also suggested to be involved in nucleic acid binding (Matias et al., 2006). However, the loops of the OB-fold structure that are likely responsible for direct contacts with DNA are unresolved in the available TIP49a structure.

The OB-fold of TIP49b is a target for the recessive *liebeskummer* mutation that causes embryonic lethality in zebrafish as a result of cardiac hyperplasia and consequent heart failure (Rottbauer et al., 2002). This mutation (*lik*-TIP49b) arises from abnormal splicing between exons 7 and 8, resulting in the in-frame insertion of three amino acids, Phe-Cys-Arg (FCR), between the conserved G190 and D191 residues of TIP49b. Isolated *lik*-TIP49b-containing complexes showed enhanced and DNA-independent ATPase activity compared to the wild-type protein as well as an altered pattern of oligomerization (Rottbauer et al., 2002). To our knowledge, how the OB-fold within the D2 domain can impact on the structure and properties of the ATP binding and hydrolysis pocket formed by the D1/D3 interface has remained uninvestigated.

Most proteins function as dynamic systems in aqueous solution, and their biologically relevant domain mobility can be described as a movement of quasi-rigid structural units (Berendsen and Hayward, 2000; Hayward, 1999; Lange and Grubmüller, 2006, 2008; Lee et al., 2003). Molecular dynamics (MD) simulation in a periodic water box is a powerful tool to investigate such large-scale protein motion at atomic resolution and can provide important information on a protein's mechanism of action. Using this approach, domain mobility can be described as the relative hinging motion of structural units around a spatially defined rotation axis. Analysis of such movements, which often involve the conformational change of only a few functionally important residues, provides a valuable resource for elucidating key principles of protein dynamics in solution (Hayward, 1999; Tyka et al., 2011).

We have analyzed the large-scale domain movements of TIP49a, TIP49b, and *lik*-TIP49b proteins in mono- and hexameric assemblies using molecular modeling and MD simulations. All follow similar key principles of conformational changes, whereby major movements are associated with the D2 domain and the C-terminal α helices of the D3 domain. In both mono- and hexameric assemblies, the D2 domain of TIP49a and TIP49b is highly flexible and does not maintain a single native conformation. This is largely confirmed by comparing all-atom models with the crystal structure of D2 domain deletions of TIP49b hexamers bound to ADP. The *lik*-TIP49b protein, however, shows an enhanced mobility of the OB-fold, collapse of the unstructured L2 loop, and unexpectedly, an increased mobility of the aa residues located at the intramolecular D1/D3 interface that forms the ATP-binding pocket. In hexamers the FCR-containing OB-folds tend to form stable intersubunit structures that most likely affect DNA binding by *lik*-TIP49b. Our results provide a rational structural and mechanistic basis for the biochemical properties of *lik*-TIP49b and suggest how its FCR insertion, which remotely affects functionally important domains of the protein, can impact both its intrinsic ATPase activity and its relative independence from DNA binding. Finally, we have extended these studies to all-atom TIP49a/TIP49b heterohexamers, allowing for important comparisons with reported heterohexameric structures that lack the OB-fold.

RESULTS

All-Atom Models of TIP49 Proteins

To investigate the large-scale conformational flexibility of TIP49 proteins, we first built all-atom models of monomeric and hexameric forms based on the crystal structure of TIP49a (PDB 2C9O) and the available NMR structure of a fragment of TIP49b (PDB 2CQA). Conformations of unstructured loops were calculated using the standard ICM-Pro protocols for loop modeling with fixed termini, yielding a variety of alternative conformations for aa residues absent in the crystal structures. The resulting lowest-energy loop structures of TIP49a are shown in Figure 1A. The unstructured L1 loop (residues 142–155) within the OB-fold adopts a β-hairpin conformation, in good agreement with the NMR structure of the OB-fold of TIP49b (see Figure S1 available online). The lowest-energy conformation of L2 (residues 248–275) was found to be a flexible structure containing two α helices separated by a loop. Because TIP49 proteins share 42% sequence identity, the TIP49b structure was homology modeled using TIP49a model as a template (Figure 1B). The resulting structures were used as initial conformations for further MD simulations of TIP49a and TIP49b proteins in mono- and hexameric form.

The Structure of TIP49b Hexamers Lacking OB-Folds

We next compared our homology-based TIP49b models with their hexameric crystal structure (PDB 3UK6) obtained using a truncated mutant lacking the OB-fold domain (TIP49bd2, a deletion of residues 131–241 replaced by the linker AGA, Figure 1C; see Table 1 and Experimental Procedures). The spatial arrangement of the D1 and D3 domains showed a good correlation between crystal and all-atom models, yielding a C-α root-mean-square deviation (RMSD) value of 2.1 Å, which decreased after 30 ns MD simulations (see below).

The TIP49bd2 crystal structure shows that the conformations and relative dispositions of the D1 and D3 domains of TIP49b in the hexamer are very similar to those reported for TIP49a (Matias et al., 2006) and the mixed TIP49a/TIP49b heterohexamer (Gorynia et al., 2011). However, our structure and results of molecular modeling highlight an important exception: the last eight amino acids of the C-terminal-most α helix, which exhibit an extended conformation in the mixed hexamers, are unstructured in

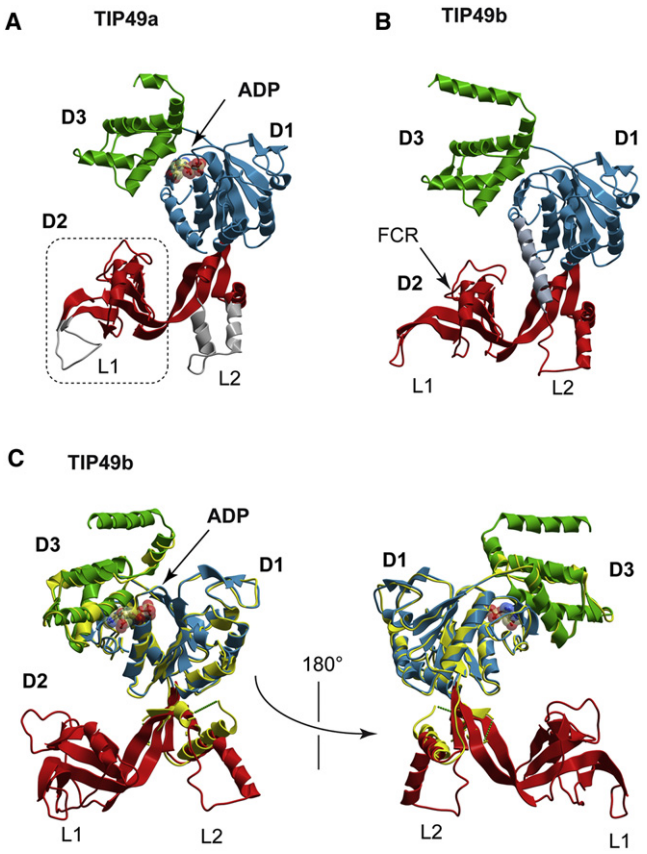

Figure 1. Spatial Structures of TIP49a and TIP49b Proteins

(A) The crystal structure of TIP49a (Matias et al., 2006) is illustrated. The D1, D2, and D3 domains are shown in blue, red, and green, respectively. Unstructured L1 and L2 loops (shown in gray) were reconstructed using the loop-modeling tools of ICM-Pro. The dotted rectangle shows the OB-fold. The ADP molecule located at the D1/D3 interface is shown (Matias et al., 2006).

(B) The homology-based spatial structure of TIP49b is presented. FCR indicates the position of insertion of the FCR triplet within the OB-fold of *lik*-TIP49b. The N-terminal α helix of TIP49b (residues 1–21) is shown in gray color.

(C) Superposition of the ADP-bound TIP49b crystal structure (shown in yellow; PDB 3UK6) on the all-atom homology model of TIP49b used in this study is demonstrated. Front and back views are shown on the left and right sides, respectively. The N-terminal α helix of the all-atom TIP49b model structure is not shown. Unresolved parts of TIP49b are shown as green dotted lines. Graphics were produced using the ICM-Pro software package.

See also Figures S1 and S2.

Table 1. Data Collection and Refinement Statistics

Space Group	$P2_1$
Unit cell	a = 113.07 Å b = 186.28 Å c = 129.86 Å α = 90.000 β = 108.953 γ = 90.000
Resolution (Å)	43.19–2.95 (3.0–2.95)[a]
Total no. of reflections	344,907
No. of unique reflections	103,557
Redundancy (%)	3.3 (3.3)
Completeness (%)	97.0 (99.2)
<I>/<s(I)>	16.74 (1.9)
R_{merge}[b] (%)	5.5 (69.3)
Refinement	
No. of protein atoms	22,540
No. of ADP atoms	322
R_{cyst}[c]/R_{free}[d] (%)	24.23/26.45
Estimated coordinate error from a Luzzatti plot (Å)	0.6
Overall B factors (Å^2)[e]	91/91/90.0
Deviations from Ideal Stereochemistry	
RMSD bonds (Å)	0.01
RMSD angles (°)	1.15
Wilson B factor (Å^2)	88.87
Ramachandran Plot Analysis[f]	
Most favored (%)	98.00
Disallowed (%)	0.27

[a]Values in parentheses are for the highest resolution shell (3.0–2.95).

[b]R_{merge}= $\Sigma(|I_i - <I>|)/\Sigma(<I>)$, where the sum is calculated over all observations of a measured reflection (I_i), and <I> is the mean intensity of all the measured observations (I_i).

[c]$R_{cryst} = \Sigma\,(|F_{obs} - F_{calc}|)/\,\Sigma\,(F_{obs})$, F_{obs} are the observed structure factor amplitudes and F_{calc} those calculated from the model.

[d]R_{free} is equivalent to R_{cryst} but where 5% of the measured reflections have been excluded from refinement and set aside for cross-validation purposes.

[e]Average B values for all atoms/protein/ADP.

[f]Ramachandran plot analysis was performed using MolProbity.

TIP49bd2. In TIP49b/TIP49a heteromeric interfaces the long C-terminal α helix of TIP49b is in direct contact with the C-terminal α helix of the adjacent TIP49a protomer, a configuration that is stabilized by interactions between a series of negatively charged residues of TIP49b (E454, E458, and D461) with positively charged residues of TIP49a (K441 and K445). In the case of the TIP49a/TIP49b interfaces, these interactions cannot occur because neutral S437 and Q441 residues of TIP49b replace K441 and K445. In addition the C-terminal helix of TIP49a is truncated at position 456 and lacks the negatively charged C-terminal series of Glu and Asp residues found in TIP49b. Of note is the observation that, in our MD simulations, the C-terminal-most TIP49a α helix can adopt alternative low-energy conformations, forming contacts with the E293 and K297 residues of the D3 domain as well as with the L365 and Y366 residues of the short loop connecting the D1 and D3 domains. These are likely to act as a hinge controlling the rotation of D3 and opening the ATP-binding site of the neighboring protomer.

The disposition of the flexible L2 loop (residues 248–275) differed between the TIP49bd2 crystal structure and the all-atom model built by homology with the TIP49a X-ray structure. L2 residues 251–253 and 268–275 were found to be in close contact with D1 (residues 113 and 117). This spatial arrangement is sterically precluded in the TIP49b model by the N-terminal α helix (residues 1–21), which forms many favorable interactions with the D1 domain in both TIP49a and TIP49b. This region is substantially disordered in the majority of monomers within the crystal structure and, at best, can only be resolved from residue 7 onward, where residues 7–21 adopt a largely extended conformation, contrary to the model and TIP49a coordinates. However,

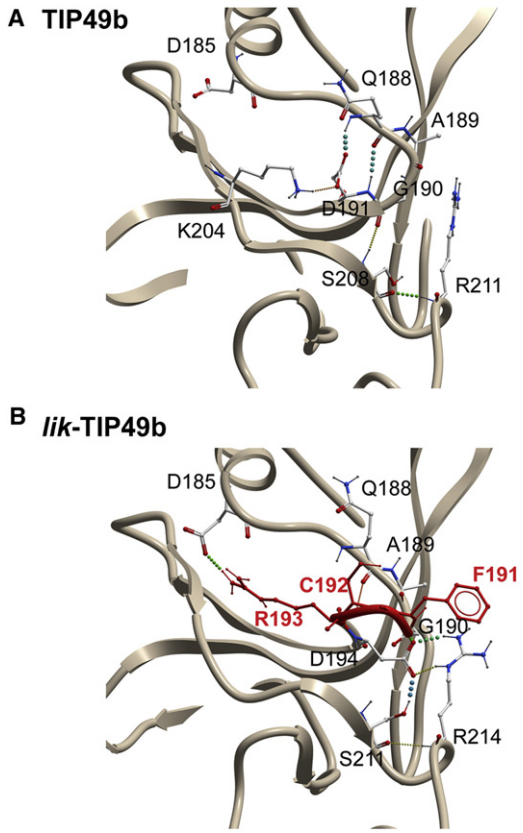

Figure 2. Effects of the FCR Insertion of *lik*-TIP49b

The effect of the FCR insertion on the OB-fold structure of *lik*-TIP49b (B) compared to the wild-type protein (A) is illustrated. The FCR insertion shown in red has been added to human TIP49b and is referred to as *lik*-TIP49b hereafter. Hydrogen bonds discussed in the text are shown as dotted lines. Because of a discrepancy with reported sequences (see http://www.uniprot.org/uniprot/Q9Y230), residues are numbered according to the UniProtKB database. See also Figure S2.

our MD simulations, described below, show that the N-terminal α helix and L2 (residues 250–273) of TIP49b are highly flexible. Accordingly, the N-terminal α helix could be displaced during the crystallization procedure, which is substantially longer than our 30 ns simulation time, and deletion of residues 131–241 may also impact on this region. Despite these differences, comparison of the crystal structure of hexameric TIP49bd2 with our homology-based data strongly supports the all-atom models of TIP49 proteins used in our study and which the analyses described below are based on.

Modeling of the *lik* Mutation of TIP49b

The *lik* mutation of zebrafish TIP49b serves as an important model for assessing the relationship between structural features and biological effects (Rottbauer et al., 2002). Accordingly, we also modeled *lik*-TIP49b by inserting FCR aa residues between the conserved G190 and D191 in the OB-fold domain of human TIP49b (Figure 2). In wild-type TIP49b (Figure 2A), this region adopts a β-turn structure due to the formation of three hydrogen bonds (H-bonds) involving the main and side chains of D191, Q188, A189, and K204. This structure is further stabilized by two H-bonds between the main chains of S208, G190, and R211 (Figure 2A), resulting in the formation of a total of five H-bonds in this region. The FCR insertion (Figure 2B) leads to a significant reorganization of the H-bond pattern that stabilizes this region. In the mutant protein, D194 (corresponding to D191 in wild-type TIP49b) forms four H-bonds with G190, R214 (R211 in wild-type TIP49b), and S211 (S208 in wild-type TIP49b), respectively; S211 and R214 also interact with each other. The inserted R193 forms additional H-bonds with D185 and Q188. As a result, the FCR insertion contributes two additional H-bonds in this region of the protein, which would be expected to lead to a local stabilization of the OB-fold structure, a prediction that could not be made based on an analysis of crystal structures lacking the OB-fold.

MD Simulations

In the TIP49 homologs the D2 domain (Figure 1) is connected to the rest of the protein via two flexible antiparallel β sheets. This feature suggests that D2 might act as an autonomous structural element with a high degree of flexibility in solution. This hypothesis was next tested using MD approaches. MD simulations of 30 ns were performed using regularized structures of TIP49 monomers and hexamers. The hydration protein model was placed in a periodic water box containing 50 mM NaCl and used to generate MD trajectories. The RMSD time courses, calculated for the C-α atoms of TIP49 proteins and determined with respect to the first MD frame obtained after solvent equilibration, demonstrate that the system became thermodynamically stable after approximately 2 ns of MD (Figure S2). TIP49a and TIP49b hexamers were subjected to the same in silico treatment and showed similar kinetics of equilibration.

Analysis of MD trajectories showed that secondary structure and overall fold topology were largely preserved in both proteins, either in mono- or hexameric form. The average backbone C-α atom RMSD showed a significantly higher backbone flexibility of monomers compared to hexamers (RMSD = $\sim$0.8 versus $\sim$0.6 nm, respectively). This is most likely due to stabilization of the conformation of the D1 and D3 domains of both proteins by additional interactions between adjacent subunits within the hexamer. High levels (>0.2 nm) of observed average C-α RMSD in the protein backbone indicate that TIP49 proteins undergo conformational changes due to large-scale domain dynamics.

Domain Flexibility in TIP49 Monomers

We next generated local flexibility maps of TIP49 monomers by calculating the drift of C-α atoms of each residue from their initial positions and plotting the resulting distances as a function of MD time (Figure 3). MD data were also used for analysis of protein large-scale flexibility, including major conformational transitions, flexible domain boundaries, and hinge and bending residues involved in this process (Table S1). This analysis illustrates the following key principles of TIP49 flexibility. In monomers the D1 domain appears to be the most stable, only showing enhanced mobility of the N-terminal α helix (Figure 3, top and middle panels). In contrast the D2 domain is intrinsically flexible and appears remarkably mobile (Movies S1 and S2 for TIP49a and TIP49b monomers). The OB-fold, including the L1 loop, shows unconstrained rotation, whereas the L2 loop shows correlated flexibility and moves as a rigid body. Consequently, the L1

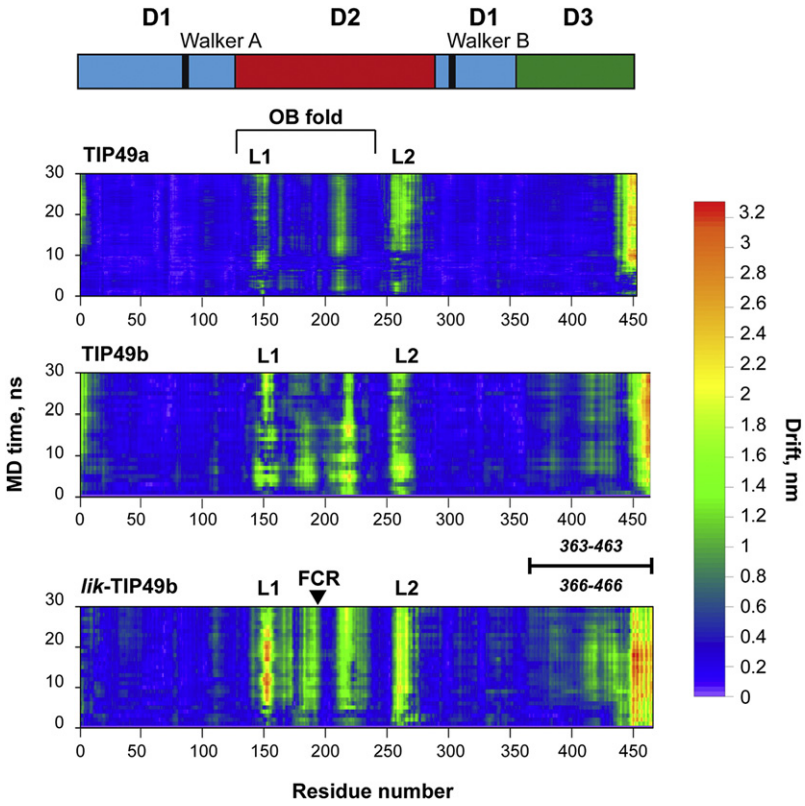

Figure 3. Local Backbone Flexibility of TIP49 Proteins

The local backbone flexibility of TIP49a (top panel), TIP49b (middle), and *lik*-TIP49b (bottom) monomers as determined by 30 ns MD simulations is presented. A schematic representation of the D1, D2, and D3 domains of TIP49 proteins (colored in blue, red, and green, respectively) is shown at the top. The color scale bar on the right represents the drift from the initial spatial position calculated for each C-α atom. The OB-fold region (indicated by the bracket) and the L1 and L2 loop positions are shown. Black vertical rectangles correspond to the Walker A and B boxes. The D3 region of *lik*-TIP49b with enhanced flexibility is indicated by a solid line above the map (bottom panel). The corresponding aa positions of TIP49b and *lik*-TIP49b are shown above and below the line, respectively. See Table S1 for the conformational analysis of TIP49 protein dynamics. See also Figures 3, S3, and S4, as well as Movies S1, S2, S3, and S8.

and L2 loops of TIP49a and TIP49b move with an amplitude >2 nm, but the OB-fold structure is retained during the 30 ns simulation time (Figure S3). Amino acids 130–131 and 229–230 of TIP49a act as bending residues that are responsible for the 23° rotation of the OB-fold domain. The high flexibility of residues 252–277 of TIP49a most probably accounts for their absence in the crystal structure (Matias et al., 2006). In TIP49b, two dynamic subregions of D2 appear to be imparted with characteristic correlated movements: residues 134–232 (OB-fold) and residues 251–275 (L2). Bending residues 131–134 and 237–240 (within the antiparallel β sheets connecting the OB-fold to the rest of the protein) together with residues 248–252 and 275–276 (connecting L2) are responsible for the 30° and 73° rotation of the OB-fold and L2, respectively. Similar to the constrained motion of D1, the mobility of D3 is restricted to its C-terminal α helices in both proteins (439–456 for TIP49a and 435–463 for TIP49b). The stable four α helices of D3 preserved their structure over the time course of the simulation, although their relative disposition was slightly changed due to the elevated flexibility of interconnecting loops. Because the ATP-binding site is located at the interface between the D1 and D3 domains, their relative rigidity is likely to be an important factor that limits or modulates the ATPase activity of TIP49 proteins. It is also important to note the existence of transient direct contacts formed between the loop spanning residues 207–220 (TIP49a) and 209–223 (TIP49b) within the OB-fold and the D3 loop spanning residues 382–383 (TIP49a), and 380–381 (TIP49b). Because the latter region is likely to be involved in the dynamics of the ATP binding and hydrolysis pocket, we expect that pocket accessibility could be affected by D2 mobility as well (see Discussion).

D2 Mobility in *lik*-TIP49b Monomers

We next applied the same approach to the *lik*-TIP49b mutation to seek a mechanistic understanding of its properties and assess the possible effects of the FCR insertion on overall domain mobility and its contribution to ATPase activity. In monomers the FCR insertion provides additional H-bonds within the OB-fold of TIP49b (Figure 2B), stabilizing the aa residues surrounding the mutation (residues 196–206; Figure 3, bottom panel). This parallels the decrease of the C-α RMSD from 8.7 to 2.1 Å in the neighboring antiparallel β sheet. Importantly, this local stabilization is accompanied by conformational changes in distant regions of *lik*-TIP49b, occurring in the domains that are likely to be responsible for DNA binding (the OB-fold and its L1 loop together with the L2 loop), and in the C-terminal part of the D3 domain.

The FCR insertion significantly affects the main OB-fold structural element, the α helix formed by residues 175–184 (Figure 4A). Over 30 ns MD simulations, the N-terminal half of this α helix unfolds and shifts away from the neighboring β-hairpin by 5–6 Å, with an angle of 29°. This changes the positions of the positively charged K177 and K184 residues that are exposed on the surface in the wild-type protein and may participate in DNA binding. Displacement of the α helix is accompanied by a rapid collapse of the unstructured L2 loop, causing it to move onto the OB-fold (Figure 4A; Movie S3). This change occurs during the first 10 ns of the MD simulation, the L2 loop of *lik*-TIP49b being retained close to the OB-fold for up to 100 ns, the maximal MD time reached during the simulation. The remarkable stability of this structure may be due to multiple favorable interactions between the OB-fold and L2. These include H-bond formation between side and main chains of K177 and G259, T202, K204, and T257 as well as hydrophobic contacts formed by the side chains of I179 and L261. Importantly, no such structures were observed in the wild-type

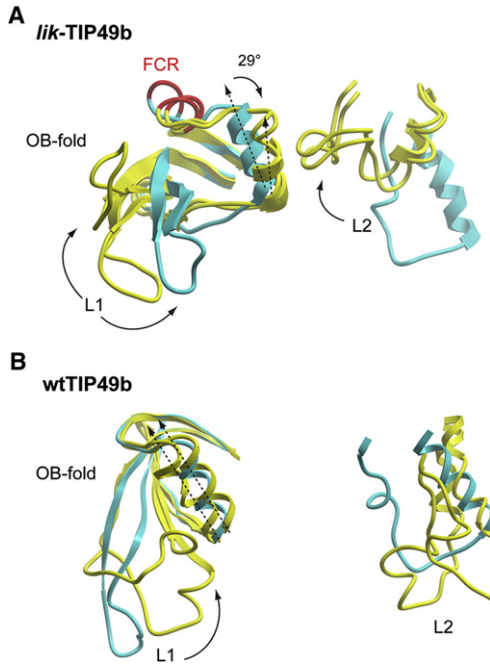

Figure 4. D2 Domain Dynamics of *lik*-TIP49b
D2 domain dynamics in the *lik*-TIP49b protein (A) are compared to wild-type TIP49b (B) as monomers. Initial conformations of the OB-fold and L2 are shown in turquoise; 10 and 30 ns conformations are shown in yellow. Dotted arrows show the central axis of the OB-fold α helix (residues 175–184); solid arrows indicate the direction of the major observed movements.

protein, the initial position of the OB-fold α helix being well preserved with respect to the OB-fold β-hairpin during the 30 ns MD simulations (Figure 4B). These observations suggest that FCR-mediated OB-fold reorganization, together with the rapid collapse of L2, should affect the DNA-binding properties of *lik*-TIP49b.

ATP Binding and Hydrolysis Pocket Dynamics in Monomers

One notable feature of the *lik* mutation is its enhanced ATPase activity (Rottbauer et al., 2002). In our MD simulations the C-terminal D3 domain of *lik*-TIP49b is significantly more flexible (Figure 3, bottom panel; residues 366–466). Because D3 acts as a lid that covers the ATP-binding pocket and traps ADP (Matias et al., 2006) (Figure 1), this increased flexibility of the D3 residues responsible for D1/D3 interface formation might account for the enhanced ATPase activity of *lik*-TIP49b. Accordingly, we calculated the surface of the ATP-binding pocket in the absence of nucleotide cofactor for all residues having direct contacts with ADP in the TIP49a crystal structure (17, 18, 20, 38–40, 42, 72–78, 366, 374, 403–404) and for the corresponding residues of the wild-type and *lik*-TIP49b proteins. The solvent-accessible surface of the ATP-binding pocket of *lik*-TIP49b was expanded during the 30 ns simulation time compared to TIP49a and TIP49b (Figure 5). This suggests that the elevated ATPase activity of *lik*-TIP49b could be due to the reduced stability of the D1/D3 interface, which consequently may increase the rate of ATP/ADP turnover.

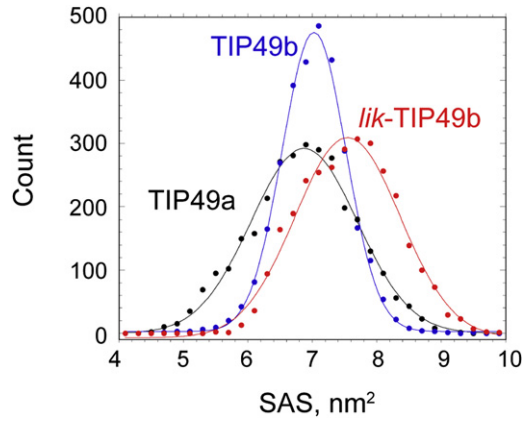

Figure 5. Surface Dynamics of TIP49 ATP-Binding Pockets
Histograms are shown for TIP49a (black), TIP49b (blue), and *lik*-TIP49b (red) monomers over the 30 ns simulation time. For each 10 ps simulation step, the solvent-accessible surface (SAS) was calculated, and the resulting data were binned to generate a histogram that was fitted to Gaussian curves using the following parameters: TIP49a, 6.9 ± 1.6 nm^2; TIP49b, 7.0 ± 0.7 nm^2; *lik*-TIP49b, 7.6 ± 1.2 nm^2 (mean ± SD). See also Table S2.

MD of TIP49 Hexamers

Whether mono- or oligomeric assemblies of TIP49 proteins constitute biologically active species remains to be clearly established. Available hexameric structures make it possible to investigate the features of domain flexibility of TIP49 assemblies that can be compared to the monomer dynamics illustrated above. Within oligomeric assemblies, domain movements of protomers are expected to be constrained because of the presence of adjacent subunit and intersubunit interactions. We indeed found this to be the case for TIP49 hexamers (Figures 6 and S4; compare to Figure 3 for monomers). Importantly, comparison of the TIP49b structure obtained after 30 ns MD simulations with the TIP49bd2 crystal structure (see Figure 1C) showed a significant decrease in C-α RMSD values, from 2.1 to 0.5 and 1.1 Å for the D1 and D3 domains, respectively. This establishes the remarkably high degree of correlation between our model and the available crystal structures. In TIP49a and TIP49b, neighboring subunits strongly stabilize the position of the D3 domain in a conformation that covers the ATP-binding pocket (Figure S4). This process involves residues 439–456, which correspond to the C-terminal α helices of D3 and form the intersubunit interface in TIP49 hexamers. Overall, D3 flexibility was reduced to that observed for the most stable D1 domain (from 25 to 2 Å), supporting the view that hexamerization of TIP49 proteins will lead to a downregulation of their ATPase activity.

D2 domains protrude from the ring structure (Figure 6; Movies S4 and S5 for TIP49a and TIP49b hexamers) without encountering any steric obstacles, and their movement was fully preserved in wild-type hexamers. MD simulations performed on TIP49b (Figures 6A and 6B) and TIP49a (Figure S3) confirm that both hexamers share similar principles of D2 flexibility. During 30 ns simulations, D2 domains adopt a variety of conformations, visible in the bottom (Figure 6B, left panel) and tilted side views (Figure 6B, right panel). The OB-fold in the A subunit, for example, protrudes out of the hexameric-ring assembly. The

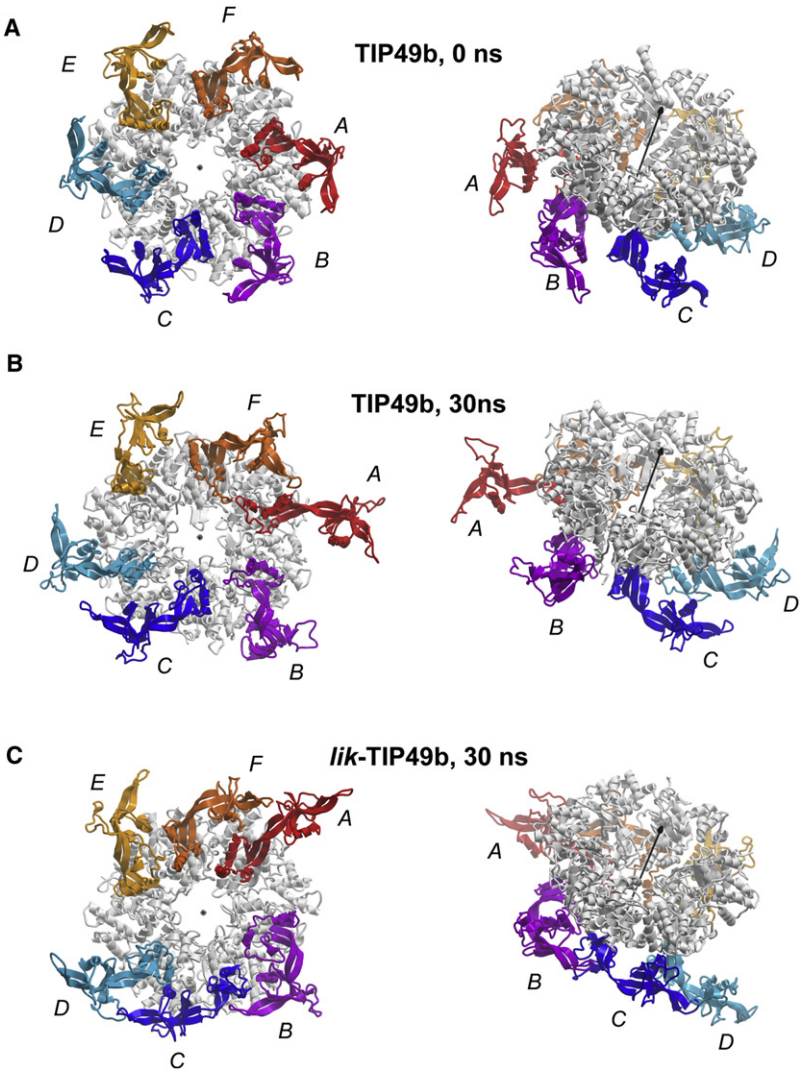

Figure 6. D2 Domain Dynamics in TIP49b Hexamers

(A) Initial bottom (left) and side (right) views of the hexamer are shown.

(B and C) D2 conformations obtained after 30 ns MD simulations for wild-type TIP49b (B) and *lik*-TIP49b (C) are illustrated. The D2 domains of each subunit are annotated alphabetically and are shown in rainbow colors. Arrows in the side views represent the central axis of the ring structure. See also Table S1, and Movies S4, S5, and S6.

OB-fold of subunit D rotates approximately 180°, such that its β-hairpin adopts an upward orientation relative to the OB-fold from the opposite subunit A, whose β-hairpin points downward. Other pairs of opposite subunits showed distinctive arrangements, highlighting the autonomous structural organization of OB-folds in wild-type TIP49 hexamers. Of note is the distinct tendency of the D2 domains in TIP49a and TIP49b hexamers to move toward and away from the oligomeric core, respectively (compare Movies S4 and S5). These results are summarized in Table S1.

These results indicate that the D2 domain of wild-type TIP49 hexamers is intrinsically flexible, whereas D1 and D3 retain their overall spatial structures. Importantly, the L1 and L2 loops of TIP49a and TIP49b retain a remarkable degree of autonomous mobility, similar to that in monomers. Additional interactions between the C-terminal α helices from neighboring subunits further stabilize the D1/D3 interfaces in hexamers compared to monomers. This suggests that hexamerization leads to the stabilization of the D1/D3 interface, most likely resulting in the complete closure of the ATP-binding pocket. The ensuing hindrance of ATP binding and subsequent release of hydrolysis products would then be accompanied by a drop in ATPase activity in TIP49 hexamers (Papin et al., 2010; Puri et al., 2007).

lik-TIP49b Domain Dynamics in Hexamers

How does the FCR insertion affect the overall organization of *lik*-TIP49b hexameric structures? We found that the D2 domains of *lik*-TIP49b hexamers form a rather stable and quasi-symmetrical arrangement (Figure 6C). In the 30 ns structures, protomers are organized in two separate groups (subunits B, C, D, and E, F, A; Movie S6). This reorganization is mediated by intersubunit van der Waals contacts between the OB-fold β-hairpins (L1) from one subunit (subunit B, for example) with different structural elements of the adjacent D2 domain (subunit C). The stable intersubunit OB-fold interactions may also restrict OB-fold rotation, which also seems to be affected in *lik*-TIP49b hexamers. Indeed, L2 collapse onto the β strand hinges (residues 134 and 240) located at the OB-fold boundaries stabilizes *lik*-TIP49 D2 domains in a conformation that most likely precludes DNA binding. The principles of *lik*-TIP49b hexamer dynamics revealed by our MD calculations are also consistent with the known biochemical properties of *lik*-TIP49b, whose enhanced ATPase activity is uncoupled from DNA binding (Rottbauer et al., 2002).

MD of TIP49 Homo- versus Heterohexamers

We next analyzed domain flexibility and MD of all-atom TIP49a/TIP49b heterohexameric assembly given the availability of the TIP49a/TIP49b crystal structure and the known biochemical properties of this complex (Figure S5; Movie S7). In contrast to wild-type TIP49 hexamers, TIP49a/TIP49b complexes showed an asymmetric pattern of interactions between adjacent protomers (Figure 7). Denoting the TIP49a and TIP49b protomers in these heterohexamers A and B, respectively, D2 domains on the ABA side (Figure 7A) form multiple intersubunit interactions between the OB-folds and L2 loops, resulting in restriction of their movements similar to that seen in *lik*-TIP49b hexamers. On the opposite side of heterohexamers, composed of BAB protomers, unconstrained D2 domain movements were fully

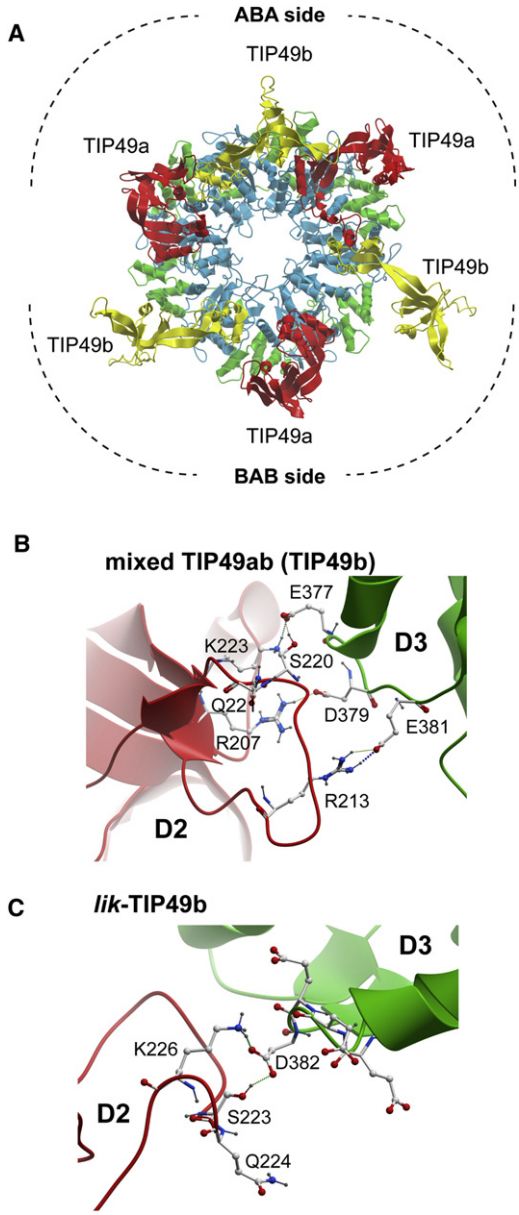

Figure 7. Inter- and Intraprotomer Rearrangements within the TIP49a/TIP49b Heterohexamer

(A) A bottom view of the hexamer after 30 ns simulation time is presented. The D2 domains of TIP49a and TIP49b are shown in red and yellow colors, respectively.

(B and C) Residues involved in the contacts between the OB-folds (red) and D3 domains of TIP49b (green) within the heterohexamer (B) and the *lik*-TIP49b homohexamer (C) are shown.

See also Figures S5 and S6, Table S2, and Movie S7.

preserved during the simulation time. The ABA side also shows direct contacts between the D2 and D3 domains of the central TIP49b protomer that further stabilize this structure (Figure 7B). These contacts involve residues 209–223 located within the OB-fold and the D3 region containing the negatively charged EEEDVD stretch of TIP49b (residues 376–381). Such rearrangements may be important for in vivo functions of TIP49 proteins: S220 of TIP49b (S223 for *lik*-TIP49b), which acts as a key residue for these interactions (Figures 7B and 7C), was identified as part of the consensus SQ/TQ sites that are recognized by ATM and ATR kinases in response to DNA damage (Matsuoka et al., 2007). Accordingly, its phosphorylation will drastically change the charge of the loop and preclude D2/D3 interactions described above, which are likely important for the downregulation of TIP49 ATPase activity by the OB-folds (Gorynia et al., 2011; Matias et al., 2006). These observations highlight the functional importance of the OB-fold, whose contributions cannot be assessed from the crystal structures of truncated proteins.

ATP-Binding Pocket Dynamics in Homo- and Heterohexamers

Results shown above highlight the profound effects of substituting TIP49a/TIP49a or TIP49b/TIP49b interfaces in homohexamers with TIP49a/TIP49b or TIP49b/TIP49a interfaces formed in heterohexamers. Because these are expected to impact ATP hydrolysis, we performed additional MD simulations of TIP49 heterohexamers lacking the OB-fold. Table S2 shows the statistical analysis of solvent-accessible surfaces for TIP49 ATP-binding pockets in the different complexes studied in our 30 ns MD simulations. One important observation is that the ATP-binding pocket of TIP49a is less accessible than that of TIP49b. However, TIP49 proteins are very weak ATPases (Gribun et al., 2008; Papin et al., 2010; Puri et al., 2007), and differences in ATP activity between TIP49a and TIP49b are very small (Gorynia et al., 2011; Gribun et al., 2008; Papin et al., 2010; Puri et al., 2007; Rottbauer et al., 2002). MD simulations showed that changes in ATP-binding pocket accessibility in wild-type TIP49a and TIP49b as well as in their mixed hexameric-ring complexes were rather small but in general agreement with available experimental data. For example a 3-fold increase in the rate of ATP hydrolysis was observed for TIP49a/TIP49b complexes deleted of their OB-folds, as compared with full-length heterohexameric TIP49 proteins (Gorynia et al., 2011; Niewiarowski et al., 2010; Puri et al., 2007). This correlates with an increase in ATP-binding pocket accessibility observed in MD simulations for mixed hexameric complexes of truncated TIP49a/TIP49b proteins (Table S2), in agreement with the increased ATPase activity of heterohexamers and dodecamers (Gorynia et al., 2011; Gribun et al., 2008; Puri et al., 2007).

By analogy to E1 and RuvB hexamers (Enemark and Joshua-Tor, 2006; Putnam et al., 2001), PDB 2GXA and 1IN4, respectively, R357 was proposed to contribute to the active site of TIP49a (R353 of TIP49b) as an R finger from a neighboring subunit (Matias et al., 2006). In regularized TIP49a and TIP49b structures modeled with ATP, Mg^{2+} and water molecules in both homo- and heterohexameric assemblies, the distance between the γ-phosphate group of ATP and polar hydrogens of R357 (TIP49a) or R353 (TIP49b) ranges from 6.3 to 7.0 Å, respectively (Figure S6). During MD simulations these arginines do not move toward ATP because of H-bond formation with D353 (TIP49a) or D349 (TIP49b) within the same protomer. Accordingly, while the hypothesis that arginines 357 and 353 of TIP49a and TIP49b proteins function as *trans*-acting R fingers is attractive, our MD simulations rule this possibility out within TIP49 hexamers. Instead, the side chain of R404 (TIP49a), which lies much closer to ADP, protrudes across the

entrance, thus trapping ADP within the binding pocket (Matias et al., 2006). In our MD simulations, R404 of TIP49a and R400 of TIP49b are found in direct contact with the β- or γ-phosphates of ATP and might act as R fingers, but in *cis*. Alternatively, arginines 404 and 400 may also be important for opening and closing the entrance of the ATP-binding pocket, allowing phosphate release for example and, thus, acting as R valves (Movie S8).

DISCUSSION

Our combined approach using homology modeling, the crystal structure of an OB-fold deletion mutant of Tip49b (Tip49b2), and the published NMR structure of this missing domain has produced a coherent framework for understanding the rules that govern the dynamic properties of the essential TIP49 proteins and of the oligomeric assemblies in which they participate. The hexameric crystal structure of TIP49bd2 not only confirms the validity of the molecular models used in our study but also provides additional information regarding the nature of the TIP49b/TIP49b interface at the atomic level. Because TIP49a and TIP49b proteins share only 42% identity at the sequence level, a direct extrapolation from the reported TIP49a and TIP49b homopolymeric complexes would have necessarily rested on unreliable assumptions.

Using MD simulations, we have also analyzed the key principles that govern the conformational flexibility and domain dynamics of these two AAA+ ATPases, in mono- and hexameric assemblies. The high degree of correlation between our all-atom models and the Tip49bd2 X-ray structure strongly supports our results. A few differences can be observed between the crystal structure and our all-atom models but tend to be relatively minor and might be attributed to the crystallization of a truncated TIP49b protein that lacks the OB-fold domain involved in large-scale domain flexibility.

In both proteins, independent of their oligomeric state, the D2 domain is intrinsically flexible. Its main movements consist of the unconstrained rotation of the OB-fold and the large-amplitude mobility of the second unstructured loop, L2, which shows correlated flexibility and moves as a rigid body. Our study also highlights the enhanced mobility of the distal C-terminal α helices belonging to the D3 domain. The core AAA+ (D1) domain appears to be the most stable and retains its overall structure up to 100 ns of MD time. The intramolecular interface formed by the D1 and D3 domains, forming the ATP binding and hydrolysis pocket, also appears to be stable and is further stabilized by the presence of neighboring subunits in the hexamer, resulting in complete closure of the ATP-binding pocket. Indeed, ADP trapping most probably renders ADP-bound TIP49 hexamers inactive molecular assemblies for ATP turnover (Matias et al., 2006; Papin et al., 2010; Puri et al., 2007). Hence, hexamerization of TIP49 proteins might constitute a mechanism for downregulation of ATP hydrolysis, fully consistent with the reported low ATPase activity of TIP49b hexamers relative to purified monomers (Elkaim et al., 2012; Papin et al., 2010). However, these data have to be reconciled with the reported failure of TIP49a monomers to form hexamers in the presence of ATP (Niewiarowski et al., 2010; Puri et al., 2007).

The embryonic lethal *lik*-TIP49b mutation described in zebrafish provides an important link to possible mechanisms that regulate ATP turnover by TIP49 proteins. Caused by the insertion of three aa residues (FCR) in the OB-fold of TIP49b, *lik* results in a gain-of-function phenotype in terms of ATP hydrolysis that somehow leads to cardiac hyperplasia and heart failure. The enhanced ATPase activity of *lik*-TIP49b-containing complexes was found to be DNA independent, suggesting that OB-fold structural alterations may also affect the DNA-binding properties of the mutant (Rottbauer et al., 2002).

The D3 α helices of *lik*-TIP49b involved in D1/D3 interface formation show a significant increase in flexibility compared to wild-type TIP49b. This results in the expansion of the ATP-binding pocket, providing a structural basis for the enhanced ATPase activity of *lik*-TIP49b, whose ATP hydrolysis rate is approximately 3-fold higher compared to wild-type TIP49b (Rottbauer et al., 2002). MD simulations also show that the FCR insertion alters the structural and dynamic properties of the D2 domain. Unconstrained OB-fold rotation, which may be an important feature of TIP49 proteins, and L2 mobility appear to be independent from each other in both the mono- and hexameric assemblies. In *lik*-TIP49b, however, OB-fold movements are altered because of the displacement of its major structural element, the α helix formed by residues 176–184. This provokes a rapid collapse of L2 onto the OB-fold, the resulting conformational reorganizations changing the positions of the positively charged surface-exposed K177 and K184 residues, which might additionally affect the DNA-binding properties of *lik*-TIP49b. Finally, in the hexameric assemblies the FCR-containing OB-folds show a trend for interactions between adjacent subunits, suggesting that within these oligomers the *lik* mutation will also serve to downregulate the DNA-binding properties of TIP49b. Because the OB-fold of TIP49a and TIP49b is also important for binding to c-Myc (Wood et al., 2000), it is likely that this domain plays crucial roles in a variety of molecular functions such as DNA and protein binding, inter- and intramolecular conformational reorganizations, and remote effects on the properties of the ATP-binding and hydrolysis pocket.

MD simulations of TIP49a/TIP49b heterohexamers show important features of the all-atom assemblies. The long extreme C-terminal α helix of TIP49b can stably interact with its counterpart in the adjacent TIP49a protomer, whereas the analogous α helix in TIP49a is found in close contact with L365 and Y366. These residues are likely to act as a hinge that controls the rotation of D3 and opening of the ATP-binding site of the neighboring protomer. In the TIP49a/TIP49b heterohexamers the OB-folds are unexpectedly reorganized in a *lik*-TIP49b-like conformation on the ABA side of hexamers, compared to the BAB side. This similarity between *lik*-TIP49b and TIP49a/TIP49b heterohexamers suggests a rational basis for the enhanced ATPase activity reported for the latter species. Taken together with our data for *lik*-TIP49b, these interprotomer OB-fold-mediated rearrangements within heterohexamers highlight the importance of another region of the TIP49 proteins: the loop spanning residues 382–383 (TIP49a) and 380–381 (TIP49b) located within the D3 domain, which may also act as a hinge in D3 domain dynamics. We also note that in some cases the D2 domains can mediate interprotein interactions between two homohexameric TIP49a and TIP49b rings, leading to the formation of dodecameric tail-to-tail TIP49a/TIP49b structures (Torreira et al., 2008). Although it would be important to perform MD simulations on these

structures, in which reduced D2 domain mobility in solution is expected to affect ATP-binding pocket dynamics, the absence of experimental data describing specific domain-domain interactions that are involved in the formation of such structures renders this task unrealistic.

Building all-atom models of TIP49 proteins and performing MD simulations on monomeric and hexameric forms, we provide a structural basis for their properties and regulation thereof. The large-scale domain flexibility we demonstrate exerts profound effects on the overall conformation of TIP49 oligomeric assemblies. Accordingly, we expect that similar principles will apply to the formation of multiprotein complexes in which TIP49 proteins have been found (see Grigoletto et al., 2011; Huen et al., 2010), where available protein/protein interaction interfaces should be subject to the same constraints. The resulting flexibility maps we provide should serve as a useful tool for the rational design of mutants and the prediction of the biological consequences of posttranslational modifications of the TIP49 proteins that play an essential role in many different aspects of nucleic acid and chromatin dynamics (Kim et al., 2007; Lee et al., 2010, 2011; Matsuoka et al., 2007). These extend to cancer pathologies in which TIP49 proteins have been implicated (Huber et al., 2008; Li et al., 2010) but for which mechanistic insights are still lacking (Grigoletto et al., 2011). We expect that such approaches will provide valuable information applicable to other biological systems in which physiological effects are largely mediated by changes in large-scale protein-domain movements.

EXPERIMENTAL PROCEDURES

TIP49b Protein Purification

Tip49bd2 was cloned, overexpressed, and purified as described in Niewiarowski et al. (2010).

Crystallization and Structure Determination

A TIP49b deletion mutation lacking residues 131–241 TIP49bd2 at a concentration of 10 mg/ml was incubated with 5 mM ADP (final concentration) for 2 hr, and the complex was used to set up several crystallization trials using commercial screens. The best crystals grew in approximately 2 days in a solution containing 0.1 M Tris-HCl (pH 8.0), 20% PEG 3000, and 5% glucose, galactose, or trehalose. These diffracted maximally to ~7.5 Å. However, the diffraction quality was significantly improved by dehydration using a barium chloride solution at 90% saturation prior to cryoprotection in 25% glycerol and flash cooling to 100° K. Data were subsequently collected at the ESRF (beamline ID-23), integrated, and scaled using XDS (Kabsch, 2010b) and XSCALE (Kabsch, 2010a), respectively. Attempts to correctly place individual molecules using a variety of Molecular Replacement packages and the available TIP49a protein coordinates for the monomer (accession code 2C9O) as a search model proved unsuccessful. However, the hexamer generated using crystallographic symmetry yielded two distinct solutions in Phaser (McCoy et al., 2007), confirming the presence of two hexamers in the asymmetric unit. Initial inspection revealed that the hexameric rings were only partially overlapping over a relatively small contact area involving the C-terminal faces of each hexamer. This arrangement is most likely to be a consequence of crystal packing. The resultant dodecamer was initially refined using PHENIX (Adams et al., 2010) following cycles of manual rebuilding in Coot (Emsley et al., 2010) and AUTOBUSTER (Bricogne et al., 2011; O.S. Smart et al., 2008, Am. Crystallogr. Assoc., abstract), where TLS refinement was also incorporated along with the use of automatically generated NCS restraints. The data collection and refinement statistics are shown in Table 1. Values for R_{work} and R_{free} are higher than would normally be expected for a similar structure refined at this resolution using the combination of PHENIX/AUTOBUSTER. This can be attributed to some of the TIP49bd2 subunits having a number of highly disordered regions. All other refinement parameters, however, are well within the expected ranges. Modeling and MD simulations were performed as described in Supplemental Experimental Procedures.

ACCESSION NUMBERS

Coordinates and structure factors for the TIP49bd2 dodecamer have been deposited in the PDB under the accession code 3UK6.

SUPPLEMENTAL INFORMATION

Supplemental Information includes six figures, two tables, eight movies, Supplemental Experimental Procedures, and Supplemental References and can be found with this article online at http://dx.doi.org/10.1016/j.str.2012.05.012.

ACKNOWLEDGMENTS

We thank the St. Petersburg State Polytechnical University and the Kurchatov Institute National Research Centre (Moscow) for allocation of computer time on multiprocessor clusters and the Center for Analytical Nano- and Biotechnology (St. Petersburg State Polytechnical University) for technical support. We thank Dave Lane for critical reading of the manuscript. This work was supported by the Federal Program of the Russian Ministry of Education and Science for invited foreign scientists (No. 02.740.11.5223 to M.G.), intramural LBME and CNRS funding (to M.G. and E.K.), and in part, by grants from the Russian Ministry of Education and Science (No 16.552.11.7037 to M.K.; Nos. 2.2.1.1.4663 and 11.519.11.2002 to M.P.) and from the Russian Academy of Science ("Physics of Elementary Particles/Studies of structure, dynamics and non-ordinary properties of matter by neutron scattering" Program).

Received: January 19, 2012
Revised: April 26, 2012
Accepted: May 26, 2012
Published online: June 28, 2012

REFERENCES

Adams, P.D., Afonine, P.V., Bunkóczi, G., Chen, V.B., Davis, I.W., Echols, N., Headd, J.J., Hung, L.W., Kapral, G.J., Grosse-Kunstleve, R.W., et al. (2010). PHENIX: a comprehensive Python-based system for macromolecular structure solution. Acta Crystallogr. D Biol. Crystallogr. *66*, 213–221.

Ammelburg, M., Frickey, T., and Lupas, A.N. (2006). Classification of AAA+ proteins. J. Struct. Biol. *156*, 2–11.

Berendsen, H.J., and Hayward, S. (2000). Collective protein dynamics in relation to function. Curr. Opin. Struct. Biol. *10*, 165–169.

Bricogne, G., Blanc, E., Brandl, M., Flensburg, C., Keller, P., Paciorek, W., Roversi, P., Sharff, A., Smart, O.S., Vonrhein, C., and Womack, T.O. (2011). BUSTER (Cambridge: Global Phasing).

Cheung, K.L., Huen, J., Houry, W.A., and Ortega, J. (2010). Comparison of the multiple oligomeric structures observed for the Rvb1 and Rvb2 proteins. Biochem. Cell Biol. *88*, 77–88.

Elkaim, J., Castroviejo, M., Bennani, D., Taouji, S., Allain, N., Laguerre, M., Rosenbaum, J., Dessolin, J., and Lestienne, P. (2012). First identification of small-molecule inhibitors of Pontin by combining virtual screening and enzymatic assay. Biochem. J. *443*, 549–559.

Emsley, P., Lohkamp, B., Scott, W.G., and Cowtan, K. (2010). Features and development of Coot. Acta Crystallogr. D Biol. Crystallogr. *66*, 486–501.

Enemark, E.J., and Joshua-Tor, L. (2006). Mechanism of DNA translocation in a replicative hexameric helicase. Nature *442*, 270–275.

Erzberger, J.P., and Berger, J.M. (2006). Evolutionary relationships and structural mechanisms of AAA+ proteins. Annu. Rev. Biophys. Biomol. Struct. *35*, 93–114.

Gorynia, S., Bandeiras, T.M., Pinho, F.G., McVey, C.E., Vonrhein, C., Round, A., Svergun, D.I., Donner, P., Matias, P.M., and Carrondo, M.A. (2011).

Structural and functional insights into a dodecameric molecular machine—the RuvBL1/RuvBL2 complex. J. Struct. Biol. *176*, 279–291.

Gribun, A., Cheung, K.L., Huen, J., Ortega, J., and Houry, W.A. (2008). Yeast Rvb1 and Rvb2 are ATP-dependent DNA helicases that form a heterohexameric complex. J. Mol. Biol. *376*, 1320–1333.

Grigoletto, A., Lestienne, P., and Rosenbaum, J. (2011). The multifaceted proteins Reptin and Pontin as major players in cancer. Biochim. Biophys. Acta *1815*, 147–157.

Hayward, S. (1999). Structural principles governing domain motions in proteins. Proteins *36*, 425–435.

Huber, O., Ménard, L., Haurie, V., Nicou, A., Taras, D., and Rosenbaum, J. (2008). Pontin and reptin, two related ATPases with multiple roles in cancer. Cancer Res. *68*, 6873–6876.

Huen, J., Kakihara, Y., Ugwu, F., Cheung, K.L., Ortega, J., and Houry, W.A. (2010). Rvb1-Rvb2: essential ATP-dependent helicases for critical complexes. Biochem. Cell Biol. *88*, 29–40.

Ikura, T., Ogryzko, V.V., Grigoriev, M., Groisman, R., Wang, J., Horikoshi, M., Scully, R., Qin, J., and Nakatani, Y. (2000). Involvement of the TIP60 histone acetylase complex in DNA repair and apoptosis. Cell *102*, 463–473.

Jha, S., and Dutta, A. (2009). RVB1/RVB2: running rings around molecular biology. Mol. Cell *34*, 521–533.

Kabsch, W. (2010a). Integration, scaling, space-group assignment and post-refinement. Acta Crystallogr. D Biol. Crystallogr. *66*, 133–144.

Kabsch, W. (2010b). XDS. Acta Crystallogr. D Biol. Crystallogr. *66*, 125–132.

Kim, J.H., Lee, J.M., Nam, H.J., Choi, H.J., Yang, J.W., Lee, J.S., Kim, M.H., Kim, S.I., Chung, C.H., Kim, K.I., and Baek, S.H. (2007). SUMOylation of pontin chromatin-remodeling complex reveals a signal integration code in prostate cancer cells. Proc. Natl. Acad. Sci. USA *104*, 20793–20798.

Lange, O.F., and Grubmüller, H. (2006). Generalized correlation for biomolecular dynamics. Proteins *62*, 1053–1061.

Lange, O.F., and Grubmüller, H. (2008). Full correlation analysis of conformational protein dynamics. Proteins *70*, 1294–1312.

Lee, J.S., Kim, Y., Kim, I.S., Kim, B., Choi, H.J., Lee, J.M., Shin, H.J., Kim, J.H., Kim, J.Y., Seo, S.B., et al. (2010). Negative regulation of hypoxic responses via induced Reptin methylation. Mol. Cell *39*, 71–85.

Lee, J.S., Kim, Y., Bhin, J., Shin, H.J., Nam, H.J., Lee, S.H., Yoon, J.B., Binda, O., Gozani, O., Hwang, D., and Baek, S.H. (2011). Hypoxia-induced methylation of a pontin chromatin remodeling factor. Proc. Natl. Acad. Sci. USA *108*, 13510–13515.

Lee, R.A., Razaz, M., and Hayward, S. (2003). The DynDom database of protein domain motions. Bioinformatics *19*, 1290–1291.

Li, W., Zeng, J., Li, Q., Zhao, L., Liu, T., Björkholm, M., Jia, J., and Xu, D. (2010). Reptin is required for the transcription of telomerase reverse transcriptase and over-expressed in gastric cancer. Mol. Cancer *9*, 132.

Matias, P.M., Gorynia, S., Donner, P., and Carrondo, M.A. (2006). Crystal structure of the human AAA+ protein RuvBL1. J. Biol. Chem. *281*, 38918–38929.

Matsuoka, S., Ballif, B.A., Smogorzewska, A., McDonald, E.R., 3rd, Hurov, K.E., Luo, J., Bakalarski, C.E., Zhao, Z., Solimini, N., Lerenthal, Y., et al. (2007). ATM and ATR substrate analysis reveals extensive protein networks responsive to DNA damage. Science *316*, 1160–1166.

McCoy, A.J., Grosse-Kunstleve, R.W., Adams, P.D., Winn, M.D., Storoni, L.C., and Read, R.J. (2007). Phaser crystallographic software. J. Appl. Cryst. *40*, 658–674.

Murzin, A.G. (1993). OB(oligonucleotide/oligosaccharide binding)-fold: common structural and functional solution for non-homologous sequences. EMBO J. *12*, 861–867.

Niewiarowski, A., Bradley, A.S., Gor, J., McKay, A.R., Perkins, S.J., and Tsaneva, I.R. (2010). Oligomeric assembly and interactions within the human RuvB-like RuvBL1 and RuvBL2 complexes. Biochem. J. *429*, 113–125.

Papin, C., Humbert, O., Kalashnikova, A., Eckert, K., Morera, S., Käs, E., and Grigoriev, M. (2010). 3′- to 5′ DNA unwinding by TIP49b proteins. FEBS J. *277*, 2705–2714.

Puri, T., Wendler, P., Sigala, B., Saibil, H., and Tsaneva, I.R. (2007). Dodecameric structure and ATPase activity of the human TIP48/TIP49 complex. J. Mol. Biol. *366*, 179–192.

Putnam, C.D., Clancy, S.B., Tsuruta, H., Gonzalez, S., Wetmur, J.G., and Tainer, J.A. (2001). Structure and mechanism of the RuvB Holliday junction branch migration motor. J. Mol. Biol. *311*, 297–310.

Rottbauer, W., Saurin, A.J., Lickert, H., Shen, X., Burns, C.G., Wo, Z.G., Kemler, R., Kingston, R., Wu, C., and Fishman, M. (2002). Reptin and pontin antagonistically regulate heart growth in zebrafish embryos. Cell *111*, 661–672.

Theobald, D.L., Mitton-Fry, R.M., and Wuttke, D.S. (2003). Nucleic acid recognition by OB-fold proteins. Annu. Rev. Biophys. Biomol. Struct. *32*, 115–133.

Torreira, E., Jha, S., López-Blanco, J.R., Arias-Palomo, E., Chacón, P., Cañas, C., Ayora, S., Dutta, A., and Llorca, O. (2008). Architecture of the pontin/reptin complex, essential in the assembly of several macromolecular complexes. Structure *16*, 1511–1520.

Tyka, M.D., Keedy, D.A., André, I., Dimaio, F., Song, Y., Richardson, D.C., Richardson, J.S., and Baker, D. (2011). Alternate states of proteins revealed by detailed energy landscape mapping. J. Mol. Biol. *405*, 607–618.

Walbott, H., Mouffok, S., Capeyrou, R., Lebaron, S., Humbert, O., van Tilbeurgh, H., Henry, Y., and Leulliot, N. (2010). Prp43p contains a processive helicase structural architecture with a specific regulatory domain. EMBO J. *29*, 2194–2204.

Wang, C.W., Chen, W.C., Lin, L.J., Lee, C.T., Tseng, T.H., and Leu, W.M. (2011). OIP30, a RuvB-like DNA helicase 2, is a potential substrate for the pollen-predominant OsCPK25/26 in rice. Plant Cell Physiol. *52*, 1641–1656.

Wood, M.A., McMahon, S.B., and Cole, M.D. (2000). An ATPase/helicase complex is an essential cofactor for oncogenic transformation by c-Myc. Mol. Cell *5*, 321–330.